Bone 127 (2019) 460–473

Contents lists available at ScienceDirect

Bone

journal homepage: www.elsevier.com/locate/bone

Full Length Article

The effects of mechanically loaded osteocytes and inflammation on bone remodeling in a bisphosphonate-induced environment

Estee L. George*, Sharon L. Truesdell, Alexandria L. Magyar, Marnie M. Saunders

The University of Akron, Olson Research Center 319, 302 E. Buchtel Ave., Akron, OH 44325-0302, USA

ARTICLE INFO

Keywords:
Bisphosphonate-related osteonecrosis of the jaw
Bone remodeling
Mechanotransduction
Mechanical load
Inflammation
Polydimethylsiloxane

ABSTRACT

Bisphosphonate-related osteonecrosis of the jaw is a disease appearing after tooth removal in patients undergoing bisphosphonate treatment for metastasizing cancers and osteoporosis. The complexity of the condition requires a multicellular model to address the net effects of two key risk factors: mechanical trauma (pathologic overload) and inflammation. In this work, a system comprised of a polydimethylsiloxane chip and mechanical loading device is used to expose bisphosphonate-treated osteocytes to mechanical trauma. Specifically, osteocytes are treated with the potent nitrogen-containing bisphosphonate, zoledronic acid, and exposed to short-term pathologic overload via substrate stretch. During bone remodeling, osteocyte apoptosis plays a role in attracting pre-osteoclasts to sites of damage; as such, lactate dehydrogenase activity, cell death and protein expression are evaluated as functions of load. Additionally, the effects of osteocyte soluble factors on osteoclast and osteoblast functional activity are quantified. Osteoclast activity and bone resorption are quantified in the presence and absence of inflammatory components, lipopolysaccharide and interferon gamma. Results suggest that inflammation associated with bacterial infection may hinder bone resorption by osteoclasts. In addition, osteocytes may respond to overload by altering expression of soluble signals that act on osteoblasts to attenuate bone formation. These findings give insight into the multicellular interactions implicated in bisphosphonate-related osteonecrosis of the jaw.

1. Introduction

The elusive disease, bisphosphonate-related osteonecrosis of the jaw (BRONJ), presents as exposed necrotic bone in the mandible or maxilla. BRONJ affects patients treated with bisphosphonates (BPs) for conditions characterized by bone loss; commonly, these are osteoporosis and bone metastases. Mechanical trauma, usually in the form of tooth extraction, and bacterial infection within the oral cavity are highly correlated with its onset [1–4]. We hypothesized that mechanical trauma and inflammation associated with infection cause a defect in bone remodeling that may contribute to BRONJ. To begin to address this complex problem, we focused on the ability of the mechanosensitive osteocytes to sense pathologic overload and relay damage signals to osteoclasts and osteoblasts within a BRONJ environment. To model the trauma of tooth extraction, we exposed BP-treated osteocytes to short-term pathologic overload via substrate stretch. Osteocyte viability as a function of trauma was evaluated and protein expression quantified. To understand the multicellular interactions implicated in BRONJ, we exposed cultures of osteoclasts and osteoblasts to osteocyte conditioned medium (CM) and quantified bone resorption and formation. To discern the role(s) of inflammation in BRONJ, we evaluated osteoclast activity in the presence and absence of inflammatory agents, lipopolysaccharide (LPS) and interferon gamma (IFN-γ). Our model is illustrated in Fig. 1. In vitro studies incorporating the multicellular interactions among the three cell types have the potential to elucidate important combinatorial effects of risk factors on bone cell activity.

1.1. Bisphosphonates

BPs are chemotherapeutical compounds that target and accumulate in the bone matrix at areas of high turnover. They act on osteoclasts to inhibit bone resorption and can lower fracture risk in osteoporotic patients. However, BPs also promote osteocyte survival, which may contribute to microcrack propagation and a decrease in the bone's mechanical integrity. Typically, osteocyte processes are severed at the site of a microcrack. Following osteocyte apoptosis, pre-osteoclasts are called to the site to resorb damaged bone and begin the repair process. However, because BPs prevent osteocyte apoptosis, pre-osteoclasts do

* Corresponding author.
E-mail addresses: eg55@zips.uakron.edu (E.L. George), slt79@zips.uakron.edu (S.L. Truesdell), alm231@zips.uakron.edu (A.L. Magyar), mms129@uakron.edu (M.M. Saunders).

https://doi.org/10.1016/j.bone.2019.07.008
Received 5 March 2019; Received in revised form 3 July 2019; Accepted 8 July 2019
Available online 10 July 2019
8756-3282/ Published by Elsevier Inc.

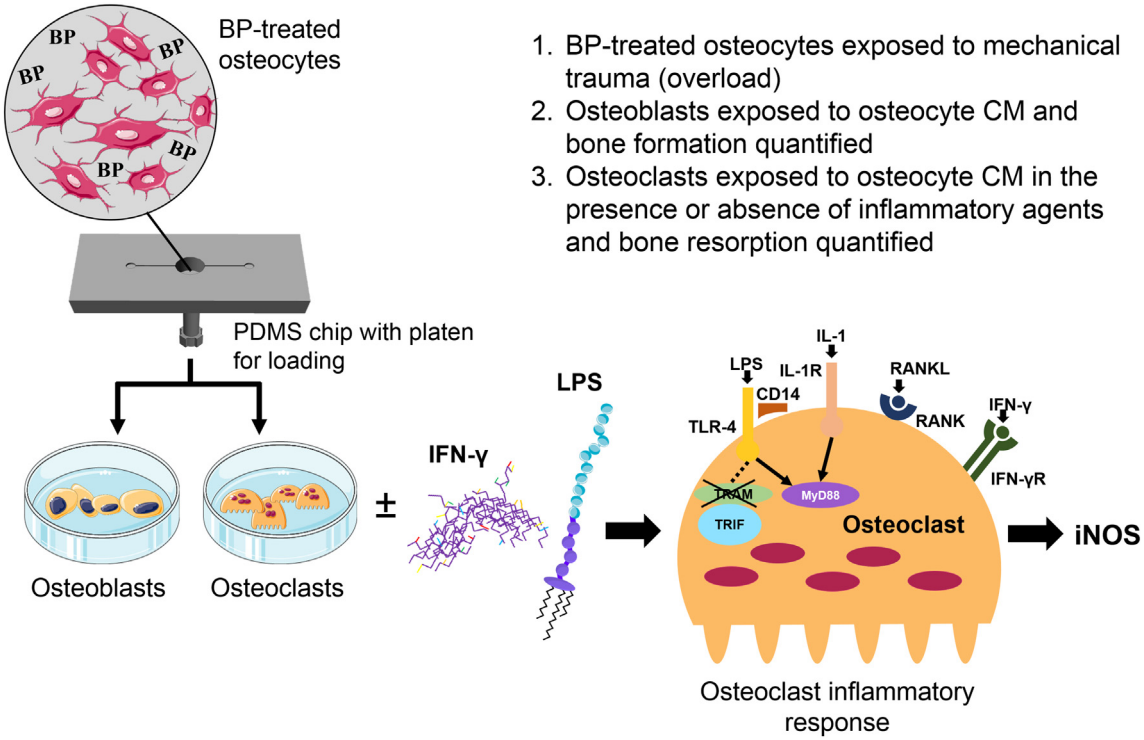

Fig. 1. Model for quantifying effects of stimulated osteocytes and inflammation on bone remodeling. Bisphosphonate (BP)-treated osteocytes are exposed to mechanical trauma (overload), and viability and secretion of soluble signals are analyzed. Osteoblasts and osteoclasts are exposed to osteocyte conditioned medium (CM), and bone formation and resorption are quantified. Osteoclasts are cultured in the presence or absence of inflammatory agents, lipopolysaccharide (LPS) and interferon gamma (IFN-γ). LPS is a pathogen-associated molecular pattern found on the outer membrane of Gram-negative bacteria. It acts on osteoclast surface protein toll-like receptor 4 (TLR-4), which uses TIR-domain-containing adapter-inducing interferon-β (TRIF) and TIR domain-containing adapter molecule 2 (TRAM) to activate interferon regulatory factors. Binding also activates nuclear factor kappa-light-chain-enhancer of activated B cells (NF-κB) by way of the myeloid differentiation primary response protein 88–dependent (MyD88-dependent) pathway [28]. Together with IFN-γ, an inducer of the Class II major histocompatibility complex, LPS promotes inducible nitric oxide synthase (iNOS) production by osteoclasts [29]. This illustration was created using images available from Servier Medical Art, which is licensed under a Creative Commons Attribution 3.0 Unported License (https://creativecommons.org/licenses/by/3.0/legalcode).

not perform this critical function [2,5]. Morphogenetic proteins are not released from the bone; this prevents osteoblast formation, which may ultimately culminate in the accumulation of necrotic bone [5,6]. However, the effects of mechanically overloaded osteocytes on bone resorption by mature osteoclasts and bone formation by osteoblasts within a BP-induced infected environment are not well understood; we seek to explain these responses.

1.2. Osteocyte strain and mechanotransduction

Strain can be categorized according to its effects on bone remodeling and/or modeling, the process by which osteoblasts mineralize to increase bone mass without prior resorption. Four strain regions exist and are termed as follows: 1) disuse, 2) adapted, 3) mild overload and 4) pathologic overload. Separating these regions are the minimum effective strains for remodeling, modeling and pathology, respectively. Bone in the adapted region undergoes remodeling, bone in the mild overload region is strengthened by a combination of remodeling and modeling and, in the pathologic overload region, woven bone formation replaces lamellar bone formation [7,8]. We seek to understand the role of osteocyte soluble factors in governing bone resorption and formation within the pathologic overload region.

Osteocytes are sensitive to a variety of mechanical stimuli, but the individual contribution of each stimulus and the molecular pathways implicated are not fully understood. You et al. suggests that osteocyte mechanotransduction may involve two distinct pathways. The first pathway is activated by fluid shear generated during moderate loading; it mediates bone adaptation and homeostasis. The second pathway is initiated by large substrate deformation that acts directly on the cells. This pathway regulates fracture healing and repair [9]. The matrix-integrin-cytoskeleton pathway may play a primary role in matrix deformation signal transduction [10]. Integrins link the extracellular matrix (ECM) and pericellular matrix (PCM) to the actin fibers and microtubules of the cytoskeleton. This provides a route for rapid signal transduction from the exterior matrices to the nucleus [11,12]. Osteocyte bodies express β1 integrins, and their cell processes express β3 integrins in a punctate pattern at attachment sites along the canalicular wall. Osteocytes are directly surrounded by PCM within their lacunae. As such, the cell bodies do not interact with lacunar walls. Instead, dendrites contact the canalicular walls at protrusions that span the PCM. Because osteopontin is concentrated along the canalicular wall, it likely serves as the ligand for αVβ3-based adhesion. It has been suggested that CD44, a receptor for osteopontin, may link tethering fibers in the pericellular space to the osteocyte cytoskeleton. Both β1 and β3 integrins may play a role in osteocyte mechanotransduction. Because tensile forces act on fibers that fasten osteocyte dendrites to the canalicular wall, load-induced fluid flow significantly increases focal strains. High stress concentrations around integrin connection sites correlate to large local deformations that initiate signaling and ATP or PGE2 release. It is less clear how strains are transmitted across the pericellular space that surrounds osteocyte cell bodies, although Nicolella et al. have suggested that large deformations can develop in the lacunar wall [13,14]. During overload, bone matrix deformation can result in high strain magnitudes of 5% or greater [9]. Eliciting bone cell responses in vitro, even at low physiologic levels, requires strain magnitudes that are substantially greater than those implicated in vivo [9,15]. This suggests that macroscopic strains are amplified at the cellular level. Bonivtch et al. developed a model to investigate the effects of the lacunar-

canicular system on osteocyte strain amplification. Results indicated that a globally applied load of 2000 microstrain can be amplified by more than a factor of three at the cellular level [16]. Our goal was to model osteocyte stretch experienced during tooth extraction. As such, an estimated average pathologic strain of ~15% was applied to a flexible polydimethylsiloxane (PDMS) membrane on which osteocytes were cultured. Due to simplification of the microstructural geometry, an amplification factor of three may be an underestimate [16]. Verbruggen et al. used confocal imaging to develop finite element studies of the lacunar-canalicular network that incorporate non-idealized models of the ECM and PCM. For the confocal image-derived models, strains observed were used to calculate a strain amplification factor of 7.7–8.9 [17].

1.3. Osteoclast inflammation

LPS is a dominant toxicity component of Gram-negative bacteria implicated in the onset and promotion of BRONJ [18]. Pathogen-associated molecular patterns, like LPS, interact with toll-like receptors (TLRs) expressed by cells of the innate immune system [19,20]. Specifically, LPS stimulates toll-like receptor 4 (TLR-4) expressed by osteoclasts deriving from the macrophage lineage. It promotes differentiation and activation by increasing receptor activator of nuclear factor-κB (RANK) signaling and cyclooxygenase-2 expression. LPS also activates the c-Jun N-terminal kinase and extracellular signal-regulated kinases 1 and 2 proliferation pathways to enhance differentiation [21]. Following stimulation, osteoclasts express pro-inflammatory cytokines including tumor necrosis factor-α, interferon-β, interleukin (IL)-1β and IL-6 as well as inducible nitric oxide synthase (iNOS) [22,23]. Kunzmann et al. have reported that the nitrogen-containing BP, pamidronate, can stimulate the secretion of IFN-γ by the Vγ9Vδ2 subset of γ/δ T cells, possibly contributing to an acute-phase reaction [24,25]. Evidence suggests that osteoclasts express IFN-γ receptor that also causes release of iNOS when stimulated [26,27] (Fig. 1). To model osteoclast response to infection within the oral cavity, osteoclasts were exposed to osteocyte CM in the presence or absence of inflammatory agents, LPS and IFN-γ.

2. Materials and methods

Fig. 2 outlines the experimental setup for this investigation. To gain insight into the effects of risk factors and multicellular interactions on BRONJ, we did the following:

1) Cultured osteocytes on PDMS chip for 72 h, treated osteocytes with BP and incubated for 24 h.
2) Induced mechanical trauma: placed PDMS chip onto loading device and stimulated osteocytes with short-term (15 min) pathologic overload via substrate stretch (15% surface strain).
3) Aspirated medium, washed cells to remove residual BP and added fresh medium to osteocytes within chip.
4) Incubated for 90 min to allow osteocytes to secrete soluble signals into medium.
5) Evaluated osteocyte viability as a function of trauma with lactate dehydrogenase (LDH) staining and annexin V and dead cell assay.
6) Collected osteocyte CM and investigated effects of soluble factors on bone remodeling. Used a cytokine array and prostaglandin E2 (PGE2) ELISA to detect and quantify proteins implicated in bone turnover.
7) Exposed cultures of osteoclasts and osteoblasts to osteocyte CM. Cultured osteoclasts in the presence or absence of inflammatory components.
8) Evaluated osteoclast activity with tartrate-resistant acid phosphatase (TRAP) stain; quantified iNOS production, TRAP activity and bone resorption.
9) Quantified osteoblast bone formation using alizarin red staining, alizarin red extraction and von Kossa staining.

2.1. Design and fabrication of PDMS chip for osteocyte culture and use with mechanical loading device

A mechanically loadable PDMS chip was developed in-house for osteocyte culture and stimulation and has been previously described [30]. It was made to enable loading of a small number of osteocytes on a deformable substrate without altering phenotype. Briefly, a mask was designed to accommodate the channel and well configuration of the chip. The arrangement was repeated eight times on a single mask for the fabrication of eight individual chips (Fig. 3a). Fig. 3b shows a side

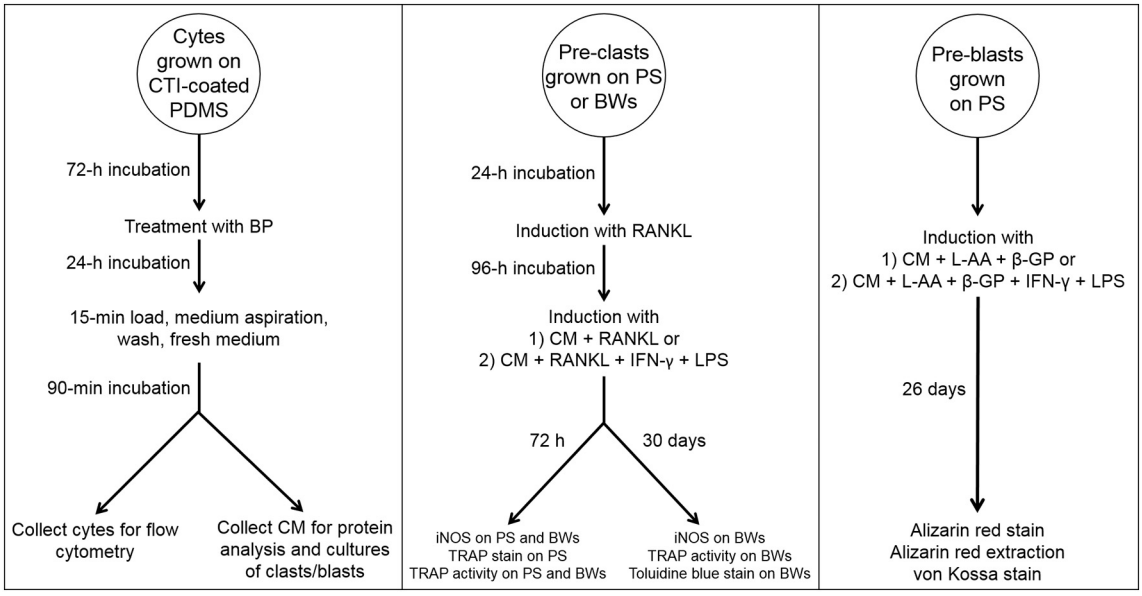

Fig. 2. Flowchart illustrating procedure and timeline for culture and stimulation of osteocytes (cytes) on polydimethylsiloxane (PDMS), pre-osteoclasts (pre-clasts) on polystyrene (PS) and bone wafers (BWs) and pre-osteoblasts (pre-blasts) on PS. To address soluble effects of short-term overload, cells were isolated by type for all studies.

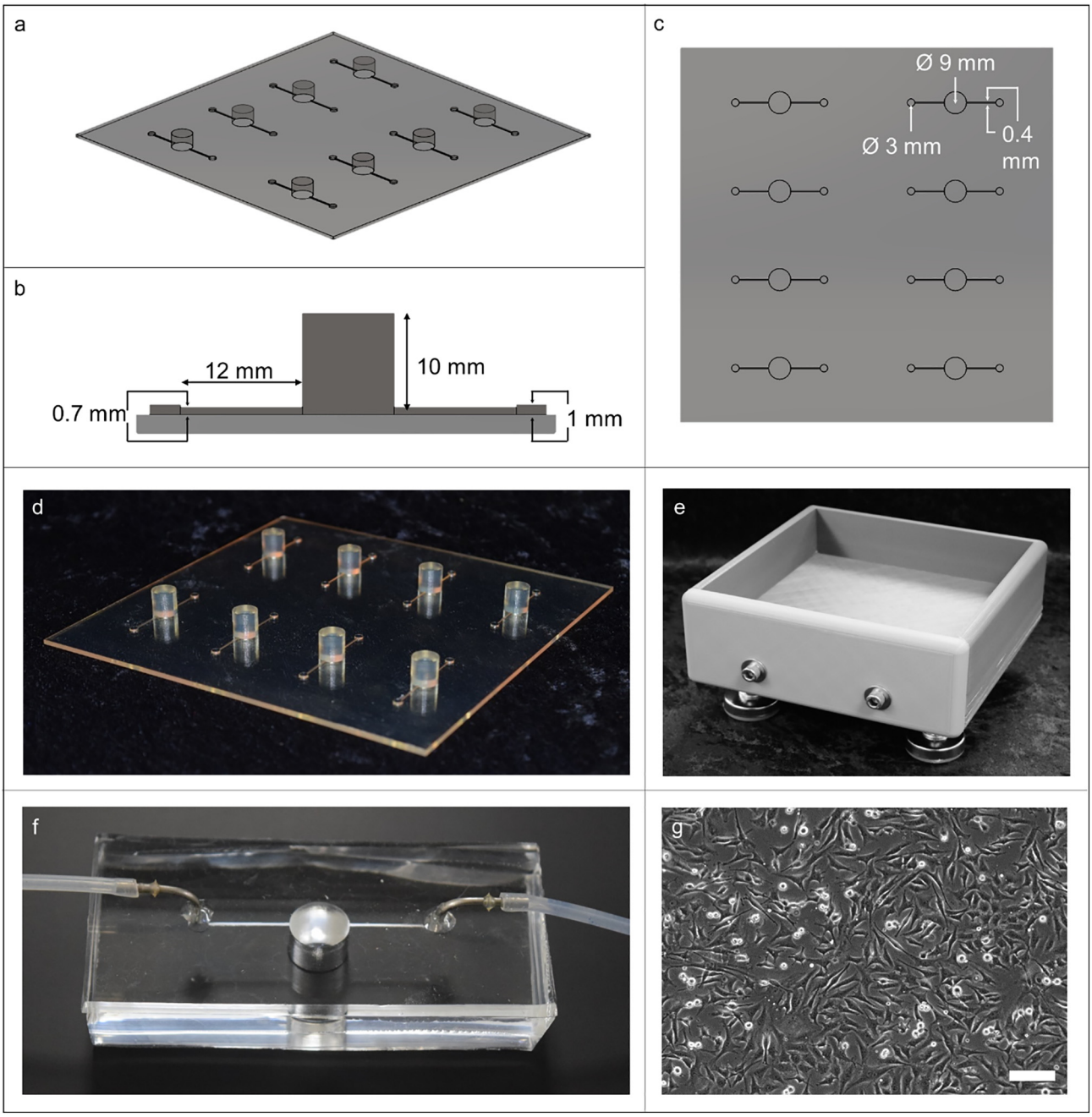

Fig. 3. Development of mechanically loadable polydimethylsiloxane (PDMS) chip. a) Mask design containing eight configurations of channels and wells. b) Expanded side view of one channel and well configuration. c) Top view of mask design. d) Photograph of mask made from Accura® SL 5530. e) 3D-printed leveling box that houses mask. f) Completed PDMS chip with angled dispensing tips and silicone tubing attached to inlet and outlet wells. g) MLO-Y4 osteocytes within chip 72 h after seeding. Scale bar measures 100 μm.

view of one such configuration and Fig. 3c shows the top view of the entire mask. The mask contains a center well for culturing osteocytes. The well created an isolated environment holding enough medium to eliminate evaporation throughout culture and testing. Two channels connect the center well to inlet and outlet wells. The mask was fabricated by Proto Labs® using Accura® SL 5530, a photopolymer resin created using stereolithography (Fig. 3d). It was placed in a leveling box (printed in-house) with leveling screws arranged in a tripod configuration (Fig. 3e).

A 10:1 elastomer base to curing agent (Sylgard 184, Dow Corning) ratio was used to make PDMS that was vigorously mixed and desiccated. PDMS was poured on top of the mask within the leveling box. It was allowed to cure overnight at 45 °C. PDMS was removed from the mask and cut into chip bases. PDMS chip lids were also fabricated using another similar leveling box that did not contain a mask. The volume of PDMS poured into the leveling box resulted in chip lids ~4.0 mm thick. PDMS chip membranes were fabricated using a third leveling box that also did not contain a mask. The volume of PDMS poured into this leveling box resulted in chip membranes 0.50 ± 0.10 mm thick. Access holes were bored through the chip lids using a biopsy punch 1 mm in diameter. PDMS bases, lids and membranes were plasma oxidized for 30 s using a medium RF power setting (Plasma Cleaner, Harrick Plasma). Plasma oxidation sterilized exposed surfaces and rendered them hydrophilic. Each base was sandwiched between one lid and one membrane. The assembled chip was baked at 45 °C for 10 min. Angled dispensing tips (18 Gauge, 0.5″, 90°) were inserted into access holes

within the chip lids and stabilized with 2-part epoxy. Tips were attached to silicone tubing (1/32″ ID). At the opposite end of each inlet tube, an 18-Gauge needle and syringe were attached. A 70% ethanol solution was pumped through each chip to sterilize the wells and channels. Ethanol was removed after 1 min, and the chips were placed under UV overnight. Chips were rinsed twice with sterile dH_2O, filled with sterile dH_2O and placed in cell culture incubators until osteocytes were ready to be seeded. A finished chip is pictured in Fig. 3f. MLO-Y4 osteocytes cultured within the chip are pictured at 72 h post-seeding (Fig. 3g).

2.2. Design and fabrication of loading device for inducing mechanical trauma

A mechanical loading device was developed to load osteocytes seeded within the PDMS chip; it has been previously described [31]. The device functions like a screw jack; a cylindrical platen is displaced in the upward vertical direction and makes contact with the underside of the PDMS membrane. Out-of-plane substrate distention creates a strain gradient on the membrane seeded with osteocytes. This substrate deformation induces osteocyte stretch. To induce pathologic overload, the membrane was subjected to an average substrate strain of ~15%. The loading device was designed to be cost-effective and to withstand high temperatures during autoclaving and humid conditions within cell culture incubators. The base of the device is shown in Fig. 4a and the underside of the device is shown in Fig. 4b.

2.3. Finite element analysis to determine strain distribution with platen displacement

The system comprised of the chip and loading device was modeled in SolidWorks 2017. Finite element analysis (FEA) was performed to characterize strains experienced by the 0.50-mm-thick PDMS membrane on which osteocytes were to be cultured; it has been previously described [31]. Briefly, the model was reduced to two components—the PDMS chip and PLA platen—and radial symmetry was used to shorten computation time. PDMS was modeled as an incompressible hyperelastic material using a two-parameter Mooney-Rivlin model for analysis. PLA was modeled as a linear isotropic material. Mesh refinement was performed for the PDMS membrane portion of the model. A convergence study was performed to determine the element size at which the average strain on the top surface of the membrane leveled off. The displacement needed to achieve an average strain of ~15% was determined. Simulations were run using membrane thicknesses of 0.50 ± 0.10 mm to ensure the maximum error in average strain was within 5% of the target strain.

2.4. Osteocyte culture and BP treatment

Results of an initial zoledronic acid (ZA) dose response suggested that a concentration of 5 μM significantly reduced osteoclast activity. An additional study was performed in which osteocytes were treated with 5 μM ZA but not loaded (data not shown). We found that TRAP activity was significantly altered when osteoclasts were exposed to resulting CM compared to CM from wells not seeded with osteocytes but treated with ZA in the same way. Taken together with a study by Scheper et al. that reported the highest concentration of ZA in saliva samples from treated patients was 5 μM, this dose was chosen for treatment [32,33].

PDMS chips were removed from the incubator and rinsed twice with sterile dH_2O using silicone tubing and a syringe. Chips were coated with collagen type I in 0.2 M acetic acid at a concentration of 5 μg/cm^2 for 1 h then rinsed twice with Dulbecco's phosphate-buffered saline (DPBS) (with calcium and magnesium). MLO-Y4 osteocytes (generously given to us by Dr. Lynda Bonewald) were seeded within the chips at a density of 15,000 cells/cm^2. They were maintained at 5% CO_2 and 37 °C for 72 h in minimum essential alpha medium (MEMα, Gibco) supplemented with 5% calf serum (CS, Hyclone), 5% fetal bovine serum (FBS, Hyclone) and 1% penicillin/streptomycin (Sigma). Cells were then treated with 5 μM ZA (Selleckchem) and incubated for 24 h.

2.5. Mechanical loading of osteocytes and collection of CM

Each PDMS chip containing ZA-treated osteocytes was placed into a holder atop the base of the loading device (Fig. 5a). The device's lid screwed into place to prevent the chip from moving during loading (Fig. 5b). The dial was rotated and platen displaced in the upward vertical direction. The device was placed in a sterile micropipette tip box and incubated (37 °C, 5% CO_2) for 15 min. The chip was removed from the loading device. Cells were washed with DPBS (without calcium or magnesium) and fresh MLO-Y4 complete medium was added. Cells were placed back into the incubator for 90 min. CM was collected using silicone tubing and a syringe; it was stored at −80 °C for no longer than 1 month. Cells were then collected for cell death analysis or stained for LDH.

2.6. LDH stain and annexin V and dead cell assay to characterize osteocyte viability as a function of trauma

For LDH staining, lids were removed from PDMS chips, and osteocytes were washed with 1× Hank's Balanced Salt Solution (HBSS, Hyclone) to remove serum. They were stained with 200 μl LDH reaction solution containing HBSS, Polypep®, diglycine, lactic acid, β-Nicotinamide adenine dinucleotide hydrate and nitroblue tetrazolium. Cells were incubated for 90 min at 37 °C and 5% CO_2. They were washed with HBSS and fixed in 4% paraformaldehyde for 15 min at room temperature (RT). They were washed again and stored in HBSS for imaging. For the annexin V and dead cell assay, lids were removed from PDMS chips and 200 μl 0.25% Trypsin-EDTA was added to each well. Osteocytes were incubated for 3 min at 37 °C and 5% CO_2, and 400 μl cell culture medium was added to each well. Cell suspensions were removed from wells, and cells were counted to ensure concentrations were between 100,000 and 500,000 cells/ml. Cell staining for the Muse™ annexin V & dead cell assay was performed in the dark and according to manufacturer's instructions. Briefly, 100 μl of each suspension was mixed with 100 μl Muse™ annexin V & dead cell reagent. Cells were stained for 20 min in the dark. Using the Muse™ cell analyzer, cells were partitioned into four populations (quadrants). The

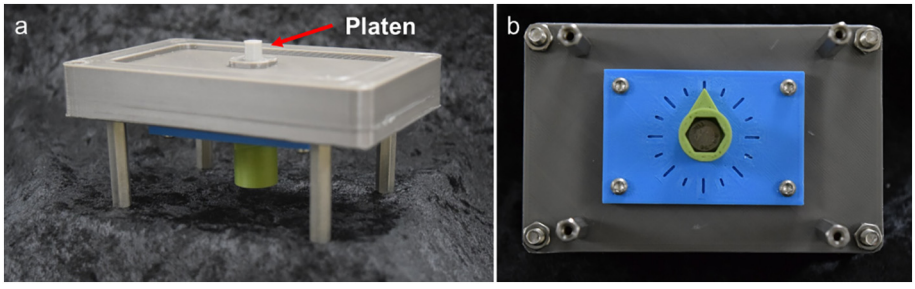

Fig. 4. Base of mechanical loading device. a) Base of loading device with raised platen visible. b) Underside of loading device showing dial and dial block. As the dial is rotated clockwise, the platen moves in the upward vertical direction. Each increment (represented by tick marks on the dial block) advances the platen 0.063 mm, applying strain to the osteocytes seeded in the polydimethylsiloxane (PDMS) chip.

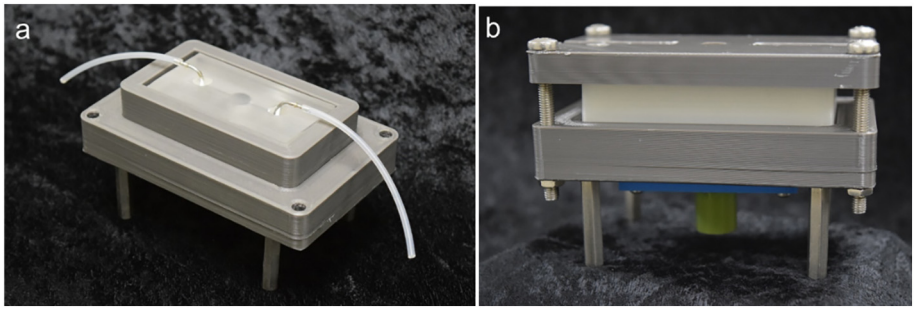

Fig. 5. Mechanical loading device. a) Polydimethylsiloxane (PDMS) chip sitting within holder of the loading device. b) Assembled loading device with lid screwed into place.

following information was determined: concentrations of viable cells, cells in the early stages of apoptosis, cells in the late stages of apoptosis or that have undergone apoptosis and necrotic cells. Percentages of cells in each quadrant, percentage of total apoptotic cells and fluorescence intensity values for populations of live and apoptotic cells were determined.

2.7. Osteocyte CM protein analysis

A cytokine analysis was performed using a quantitative sandwich-based array (QAM-CAA-4000, RayBiotech, Norcross, GA, USA). Cytokines in each CM sample were detected by a fluorescence laser scanner and concentrations determined. Additionally, an ELISA for the quantification of PGE2 was performed using the Parameter™ PGE2 Assay (R&D Systems). Steps were performed according to manufacturer's instructions. Briefly, particulates from each CM sample were removed by centrifugation. Each sample was diluted by 3-fold and assayed in triplicate. After pipetting samples into appropriate wells of a 96-well microplate, primary antibody solution was added. The microplate was covered with a plate sealer and incubated for 1 h at RT on a shaker. PGE2 conjugate was added; the microplate was covered with a plate sealer and incubated for 2 h at RT on a shaker. Each well was aspirated and washed four times with wash buffer. Substrate solution was added to each well, and the microplate was incubated for 30 min at RT, protected from light. Stop solution was added, and the optical density was determined for each well. Microplate readings were taken at 450 and 540 nm. Readings at 540 nm were subtracted from readings at 450 nm to adjust for optical flaws in the plate. The concentration of PGE2 in each sample was determined.

2.8. Osteoclast culture and inducing inflammation

In preliminary work, studies were performed to determine whether to induce inflammation in osteoclast cultures using LPS or LPS in combination with IFN-γ. Dose responses were carried out to determine the concentration of each to use for stimulation (data not shown). Based on this work and published data, concentrations of IFN-γ ranged from 8 to 80 U/ml and concentrations of LPS from 10 to 100 ng/ml [34]. Osteoclast production of iNOS and TRAP activity were quantified. A combination of 80 U/ml IFN-γ and 100 ng/ml LPS were ultimately chosen for stimulation based upon significantly altered iNOS production and TRAP activity. RAW 264.7 pre-osteoclasts (ATCC) were seeded onto tissue culture treated polystyrene or bovine bone wafers (boneslices.com) within 96-well plates. They were seeded at a density of 5,000 cells/ml in Dulbecco's Modified Eagle Medium (DMEM, Corning) supplemented with 10% FBS and 1% penicillin/streptomycin. Cells were maintained at 5% CO_2 and 37 °C. At 24 h post-seeding, cells were induced to undergo osteoclastogenesis with 120 ng/ml receptor activator of nuclear factor-κB ligand (RANKL, R&D Systems) in cell culture medium. After 96 h, cells had matured into multinucleated osteoclasts; cell culture medium was aspirated and replaced with 1) 50% standard medium + 50% CM containing 120 ng/ml RANKL or 2) 50% standard medium + 50% CM containing 120 ng/ml RANKL, 80 U/ml IFN-γ (Miltenyi Biotec) and 100 ng/ml LPS purified from the enterobacteria, *Salmonella typhosa* (Sigma). Osteoclasts were fed every 48 h by 50% volume replacements. To determine short-term response of osteoclasts and given their short lifespan on polystyrene, cells cultured on polystyrene were analyzed after 72 h. Osteoclasts cultured on bone wafers have a longer lifespan and resorb bone within 20–30 days in our hands. To determine the short- and long-term response of osteoclasts on bone wafers, analyses were performed after 72 h and 30 days.

2.9. Analyses of osteoclast iNOS production, TRAP activity and bone resorption

The concentrations of iNOS produced by osteoclasts were determined using a Griess assay. Fifty microliters of each sample was added to 50 µl of Griess reagent—a solution containing 0.5% sulfanilamide, 0.05% N-(1-Naphthyl)ethylenediamine dihydrochloride and 2.5% phosphoric acid. The absorbance at a wavelength of 540 nm was determined for each sample using a plate reader. Absorbance values were converted to concentrations of iNOS. For analysis of TRAP activity, osteoclasts were fixed using 10% neutral buffered formalin (NBF). A 1:1 acetone:methanol solution was added to each well; after 3 min, the solution was removed and wells were dried for 1 min. TRAP activity substrate—a solution containing sodium acetate, sodium tartrate and *p*-Nitrophenyl phosphate—was added to each well. Following a 60-min incubation at 37 °C, 100 µl TRAP activity substrate from each well was added to 50 µl 1 M NaOH. The absorbance at a wavelength of 405 nm was determined for each sample using a plate reader. Following fixation with 10% NBF, TRAP stain—a solution containing fast garnet, sodium nitrite, naphthol, tartrate and acetate—was added to each well. Samples were incubated at 37 °C for 60 min, washed and imaged. For toluidine blue staining, osteoclasts were removed from bone wafers by sonicating in 70% isopropanol for 30 min and gently cleaning with cotton swabs. Wafers were submerged in toluidine blue solution for 5 min, washed and dried, then submerged in toluidine blue solution for another 2 min. Wafers were washed and dried, then imaged. The percentage of area resorbed was determined for each wafer using ImageJ.

2.10. Osteoblast culture

MC3T3-E1 pre-osteoblasts (ATCC) were seeded onto tissue culture-treated polystyrene within 96-well plates at a density of 2500 cells/cm^2 in MEMα supplemented with 10% FBS and 1% penicillin/streptomycin. Cells were maintained at 5% CO_2 and 37 °C. After 5 days, cells were 100% confluent. Cell culture medium was aspirated and replaced with 50% standard medium + 50% CM; 50 µg/ml L-ascorbic acid (L-AA) and 10 mM β-glycerophosphate (β-GP) were added. Cells were fed every 72 h by 50% volume replacements. In our hands, osteoblasts form bone within 26 days; thus, analyses were performed after 26 days.

2.11. Visualization and quantification of osteoblast bone formation

For alizarin red staining, osteoblasts were fixed using 10% NBF. A 58.4 mM solution of alizarin red was added to each well, and the cells were incubated at 37 °C for 30 min in the dark. The alizarin red solution was removed, and cells were washed four times (each time for 1 min) with dH_2O. Wells were imaged, and the areas covered by stain were determined using ImageJ. A 10% acetic acid solution was added to each well of osteoblast cultures previously stained with alizarin red. Plates were incubated overnight (RT) on an orbital shaker (200 rpm). Samples were scraped from the bottom of wells and transferred into microcentrifuge tubes. They were heated at 85 °C for 10 min and transferred to ice for 5 min. They were centrifuged at 18,000 × *g* for 20 min. Supernatant for each sample was collected. Absorbance at a wavelength of 405 nm was determined for each supernatant sample and concentration calculated. For von Kossa staining, osteoblasts were fixed using a 4% paraformaldehyde solution. A 5% solution of silver nitrate was added to each well, and cells were incubated at RT for 25 min under UV light. After staining, the silver nitrate solution was removed and cells were washed three times (each time for one min) with deionized H_2O. Wells were imaged and areas covered by stain determined using ImageJ.

2.12. Statistics

With the exception of cytokine array data, all data were summarized by means with standard errors of the means and bar charts. D'Agostino-Pearson tests determined normality. Parametric data were analyzed using a *t*-test or one-way analysis of variance (ANOVA) with Tukey's test. Nonparametric data were analyzed using a Mann-Whitney test or Kruskal-Wallis test with Dunn's Multiple Comparison test. For all tests, 95% confidence intervals were used. Experiments were conducted a minimum of three times in triplicate. For the cytokine array, three samples of CM from each group (control and experimental) were spotted four times per protein. This provided twelve data points but represented three true replicates. For some proteins, all samples within one group contained concentrations below or near the limit of detection (LOD). In addition, all samples in the comparative group contained protein concentrations well above the LOD. For these cases, a conservative statistical analysis was performed by substituting the low sample concentrations with the LOD. The standard deviation was assumed the same as the standard deviation of the comparative group. Two-tailed *t*-tests were performed to determine significance, and 95% confidence intervals were used.

3. Results and discussion

3.1. Finite element analysis to determine strain distribution with platen displacement

To determine the platen displacement needed to achieve an average strain of ~15% on the top surface of the PDMS membrane, FEA was performed. Results indicated that this strain converged at an element size of 250 μm; thus, 250-μm elements were used. Surface strains were plotted against displacement, and a trend line was generated (Fig. 6a). From the equation of the trend line, it was determined that a displacement of ~1.84 mm would result in a surface strain of ~15%. A simulation was run using this displacement for verification. A color map illustrating strain distribution resulting from a displacement of 1.84 mm is shown in Fig. 6b. Simulations using membrane thicknesses of 0.40 mm and 0.60 mm indicated that an average strain of 15 ± 0.6% could be achieved for all chips with a platen displacement of ~1.84 mm.

3.2. LDH stain and annexin V and dead cell assay to characterize osteocyte viability as a function of trauma

Representative images of loaded (experimental) and non-loaded (control) osteocytes stained for LDH are shown in Fig. 7. Circular images show entire bottom surfaces of PDMS wells (9 mm in diameter). Rectangular images show an area in the center, an area between the center and rim and areas at the rim of each well. A distinct difference in stain intensity can be seen between the two groups; loaded cells stained less intensely than did non-loaded cells. Fig. 8a shows the percentages of early apoptotic, late apoptotic/dead and total apoptotic cells for each group; Fig. 8b shows the percentage of necrotic cells for each. While there were no statistically significant differences in cell death between the groups as indicated by the annexin V and dead cell assay, the following trends were observed: 1) a higher percentage of cells in the experimental group were in the early stages of apoptosis, 2) a lower percentage of cells in the experimental group were undergoing apoptosis or had died via apoptosis, and 3) a higher percentage of cells in the experimental group had died via necrosis. Taken together with the qualitative results of LDH staining, it may be that BP-treated osteocytes stimulated with short-term overload tend to die via necrosis. While it has been suggested that LDH release is indicative of necrosis (it leaks through permeabilized cell membranes), multiple additional assays are required to exclude apoptosis as the primary mechanism of death [35,36].

3.3. Osteocyte CM protein analysis

Results of the cytokine array analysis are given in Tables 1–3. The cytokines for which concentration increased or decreased significantly with load are presented in Table 1. The cytokines for which concentrations increased or decreased insignificantly are presented in Tables 2 and 3, respectively. Percent increases or decreases with load are given and presented using a color scale. Finally, a PGE2 ELISA indicated that osteocytes stimulated with short-term overload produced 64.09% more PGE2 than did non-loaded osteocytes (data not shown).

Results suggest that experimental conditions significantly decrease osteocyte expression of CCL21 and CD36 and increase expression of leptin, osteonectin and PGE2. To explain the implications of these changes requires investigation into the isolated and combinatorial effects of these proteins on cellular interactions and functional activity. CCL21 promotes osteoclast migration and resorption [37]. It is reasonable to expect that a decrease in its expression may prevent osteoclast migration to the site of trauma and removal of damaged matrix. Kevorkova et al. demonstrated that trabecular bone in CD36 knockout mice displays an osteopenic phenotype which may be associated with altered osteoblast function and hindered bone formation [38]. Contrastingly, Koduru et al. reported that CD36 knockout mice show increased trabecular bone mass. Their findings support roles for CD36 in aiding osteoclastogenesis and, together with CD47, promoting bone resorption. Their work also supports a role for CD36 in the suppression of nitric oxide synthesis by thrombospondin-1. This is important, as decreased nitric oxide levels have been shown to induce osteoclastogenesis and bone resorption [39,40]. Interestingly, Schroeder et al. reported that platelet-rich plasma can inhibit osteogenesis during craniofacial bone repair and that this restriction is associated with an increased presence of CD36+ cells [41]. Elefteriou et al. explained that leptin regulates bone resorption by antagonistic pathways. They showed that leptin is involved in sympathetic signaling, which promotes osteoclast differentiation and resorption and decreases bone formation via β2-adrenergic receptors present on osteoblasts. However, leptin also controls expression of cocaine amphetamine regulated transcript, which inhibits osteoclast differentiation and resorption [42]. Interestingly, leptin induces suppressor of cytokine signaling-3 (SOCS3), which inhibits cytokine signaling and regulates the response of macrophages to cytokines. However, ZA prevents SOCS3

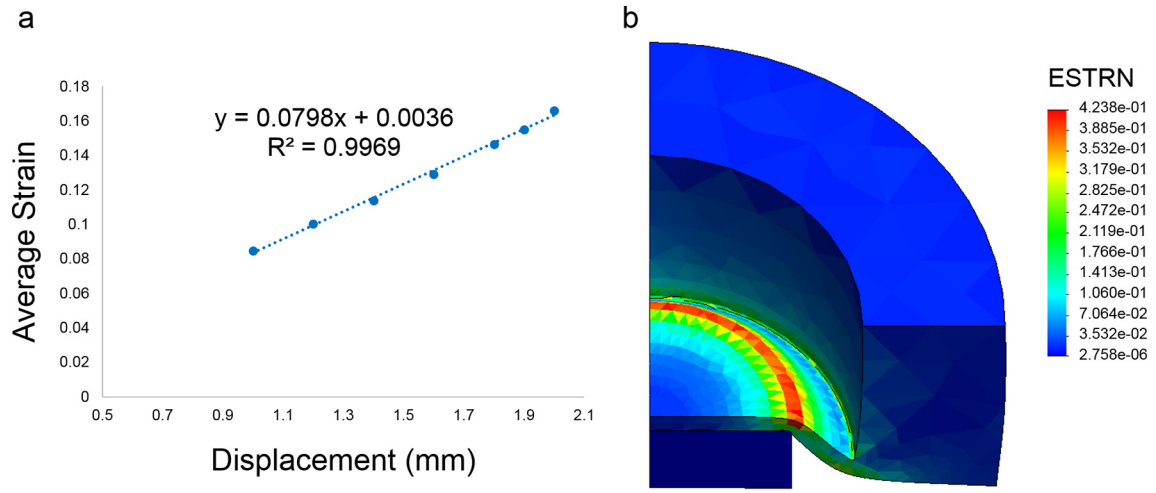

Fig. 6. Results of finite element analysis (FEA). a) Graph showing average strain on top surface of polydimethylsiloxane (PDMS) membrane versus platen displacement. The equation of the trend line and corresponding R^2 value are shown. b) Color map of strain distribution on membrane using a platen displacement of 1.84 mm. Warmer colors represent larger strains, and cooler colors represent smaller stains.

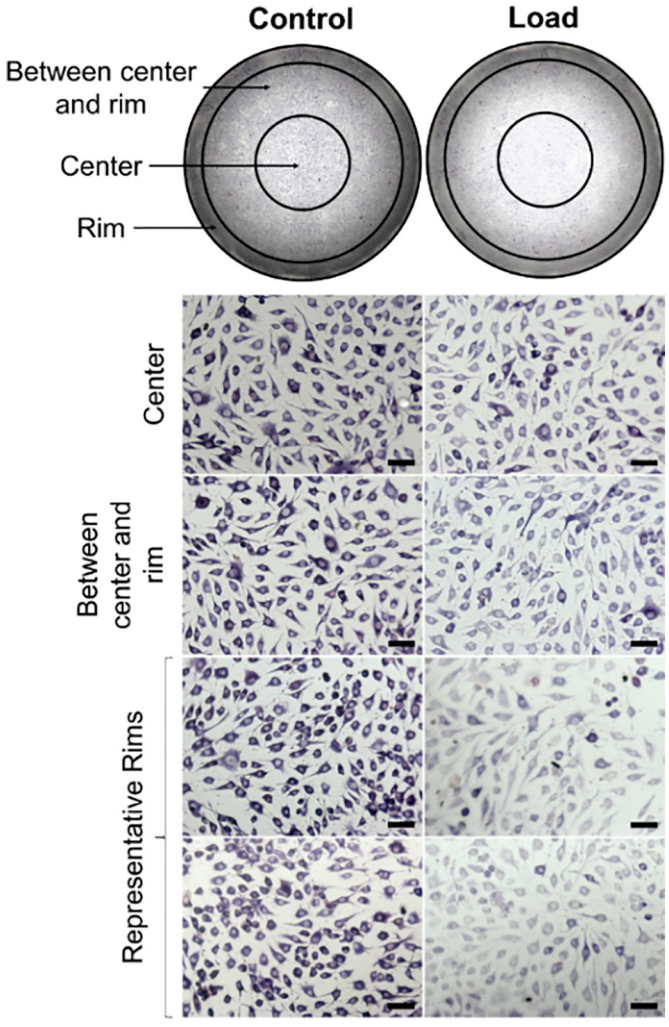

Fig. 7. Lactate dehydrogenase (LDH) stains. Top: whole-well images of control (left) and loaded (right) osteocytes stained for LDH. Bottom: Representative images of LDH-stained osteocytes at three locations within well (center, between center and rim, rim). Scale bars measure 50 μm.

accumulation in macrophages. Scheller et al. propose that SOCS3 inhibition and deregulation of cytokine production by macrophages may support the pathogenesis of ZA-induced osteonecrosis of the jaw [43]. The matricellular protein, osteonectin, is critical for the preservation of bone mass and quality; it balances formation and resorption in response to parathyroid hormone. It promotes osteoblast differentiation, survival and mineralization [44–46]. Osteonectin also plays a role in maintaining the integrity of collagen fibers in the periodontal ligament (connective tissue that anchors tooth cementum into the bone). Rosset et al. reported that the periodontal ligament of mice lacking osteonectin showed reduced amounts of total collagen and thin fiber content. They also indicate that the force required for tooth extraction was significantly decreased in these mice [47]. Finally, PGE2—released by osteocytes in response to mechanical stimulation—is implicated in the bone's response to trauma. It acts through membrane receptors to control osteoclast and osteoblast differentiation as well as to promote normal bone resorption and formation for maintaining homeostasis [48]. We also report differential changes in expression of several other chemokines with overload, but no statistically significant differences were observed.

3.4. Analyses of osteoclast iNOS production, TRAP activity and bone resorption

Results of the Griess assay are presented in Fig. 9. For osteoclasts cultured on polystyrene for 72 h post-stimulation, iNOS was only produced in the presence of inflammatory agents (Fig. 9a). When cultured on bone wafers for the same amount of time, osteoclasts exposed to only experimental CM also produced iNOS. Osteoclasts exposed to inflammatory agents and control CM produced ~300% more iNOS than did osteoclasts exposed to experimental CM. Osteoclasts exposed to inflammatory agents and experimental CM produced ~300% more iNOS than did osteoclasts exposed to only experimental CM (Fig. 9b). Fig. 9c illustrates the following results corresponding to culture on bone wafers for 30 days post-stimulation: 1) osteoclasts exposed to inflammatory agents and control CM increased iNOS production by 193.3% over osteoclasts stimulated with experimental CM, 2) osteoclasts exposed to inflammatory agents and control CM increased iNOS production by 156.7% over osteoclasts stimulated with only control CM, 3) osteoclasts exposed to inflammatory agents and experimental CM increased iNOS production by 214% over osteoclasts stimulated with only experimental CM, 4) osteoclasts exposed to inflammatory agents and experimental CM increased iNOS production by 174.8%

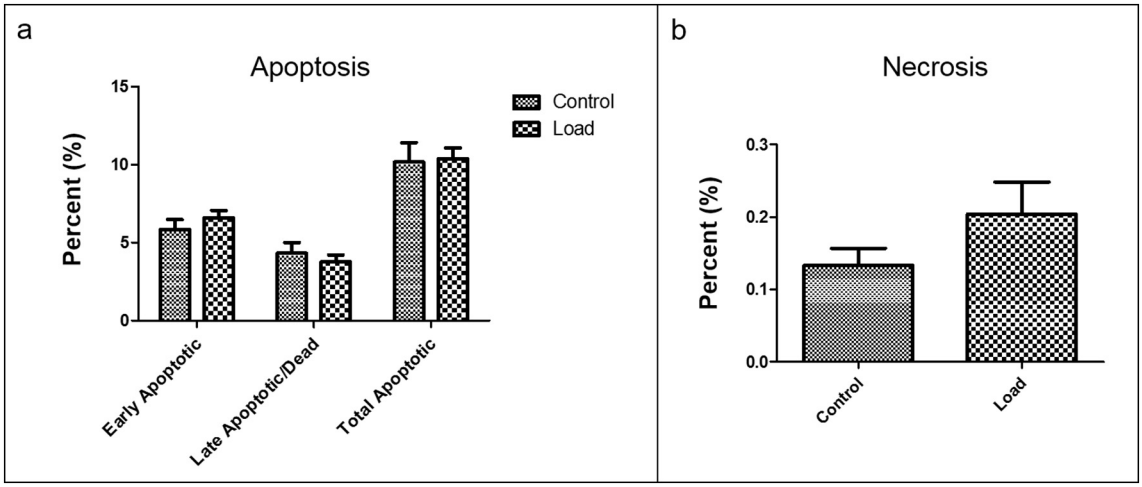

Fig. 8. Results of annexin V and dead cell assay. a) Percentages of control and loaded osteocytes in early and late apoptotic phases of cell death. b) Percentages of necrotic control and loaded osteocytes.

over osteoclasts stimulated with control CM. As expected, these results suggest that osteoclasts exposed to inflammatory agents produce more iNOS than osteoclasts not exposed to inflammatory agents. Results also indicate that soluble factors from osteocytes exposed to short-term overload do not alter iNOS production.

Representative images of osteoclasts stained for TRAP are shown in Fig. 10a. These cells were grown on polystyrene and exposed to control or experimental CM in the presence or absence of inflammatory agents. Cells were stained and images taken 72 h post-stimulation. Fig. 10b illustrates the following results corresponding to culture on polystyrene for 72 h post-stimulation: 1) osteoclasts exposed to inflammatory agents and control CM showed 36.0% less TRAP activity than did osteoclasts exposed to experimental CM, 2) osteoclasts exposed to inflammatory agents and experimental CM showed 35.1% less TRAP activity than did osteoclasts exposed to only experimental CM, 3) osteoclasts exposed to inflammatory agents and control CM showed 36.7% less TRAP activity than did osteoclasts exposed to only control CM, 4) osteoclasts exposed to inflammatory agents and experimental CM showed 35.9% less TRAP activity than did osteoclasts exposed to control CM. Fig. 10c illustrates that when cultured on bone wafers for 72 h post-stimulation, osteoclasts exposed to inflammatory agents and control CM showed 14.8% less TRAP activity than did osteoclasts exposed to experimental CM. Osteoclasts exposed to inflammatory agents and control CM showed 14.5% less TRAP activity than did osteoclasts exposed to only control CM. Interestingly, Fig. 10d shows a dissimilar trend for osteoclasts cultured on bone wafers for 30 days post-stimulation. Results indicate the following: 1) osteoclasts exposed to inflammatory agents and control CM showed 295.3% more TRAP activity than did osteoclasts exposed to experimental CM, 2) osteoclasts exposed to inflammatory agents and control CM showed 124.4% more TRAP activity than did osteoclasts exposed to only control CM, 3) osteoclasts exposed to inflammatory agents and experimental CM showed 219.6% more TRAP activity than did osteoclasts exposed to only experimental CM.

Representative images of bone wafers stained with toluidine blue are shown in Fig. 10e. Osteoclasts were grown on bone wafers; they were cultured in the presence or absence of inflammatory agents and exposed to control or experimental CM. Bone wafers were stained and images taken 30 days post-stimulation. The percentage of surface area resorbed was quantified for each bone wafer. It is important to note that one bone wafer within the "load" group showed little to no resorption. While no obvious issues were observed, cells cannot be visualized on bone wafers. As such, we were unable to verify cell health and anchorage to the bone wafer. We do not believe this sample represents osteoclast activity under experimental conditions. Thus, the graph in Fig. 10f was generated with this outlying data point excluded. Osteoclasts exposed to inflammation in addition to experimental CM resorbed 42.6% less surface area than did osteoclasts exposed to control CM; they resorbed 45.2% less surface area than did osteoclasts exposed to experimental CM. Also, osteoclasts exposed to inflammation in addition to control CM resorbed 41.1% less surface area than did osteoclasts exposed to experimental CM. These results were unexpected given that opposite trends were observed for TRAP activity by the same osteoclasts.

In summary, we found that osteoclasts exposed to LPS and IFN-γ increase iNOS production and that the addition of soluble factors from loaded osteocytes does not modify this response. Osteoclasts on both substrates (polystyrene and bone wafers) showed decreased TRAP activity in response to LPS and IFN-γ at 72 h. However, osteoclasts on bone wafers showed increased TRAP activity in response to LPS and IFN-γ at 30 days. These same osteoclasts resorbed less bone than did osteoclasts not exposed to LPS and IFN-γ. This may be explained by the fact that TRAP can be present in osteoclasts in an inactive pro-form. Activation by proteinases is required for its participation in bone degradation [85,86]. Additionally, as more TRAP is produced at an early time point (72 h), it may be that resorption is instigated early on and tapers off by 30 days. It is important to note that TRAP activity, in general, decreased by 30 days, as indicated by the difference in y-axis scales between Fig. 10c and d. Finally, neither TRAP activity nor resorption were altered by the addition of soluble factors from loaded osteocytes. Under these experimental conditions, osteoclasts are more

Table 1
Osteocyte cytokines for which concentration changed significantly with load.

	Role in osteoclast/osteoblast activity	Change with load
CCL21	Promotes osteoclast migration and resorption [37,49]	−85.43%
CD36	Ensures adequate mineralization [38]; supports osteoclast formation and resorption [40]	−40.16%
Leptin	Involved in sympathetic signaling, which promotes osteoclast differentiation and resorption and decreases bone formation via Adrb2; controls expression of CART, which inhibits osteoclast Differentiation and resorption [42]	33.54%
Osteonectin	Promotes osteoblast differentiation, survival and mineralization [44,45]	8.88%

Table 2
Osteocyte cytokines for which concentration increased insignificantly with load.

	Role in osteoclast/osteoblast activity	Change with load
IL-17F	Promotes osteoblast differentiation [50]	1.06%
OPN	Promotes osteoclastogenesis and osteoclast activity, mediates osteoclast survival, podosome formation and motility; inhibits osteoblast mineralization [51]	5.40%
VEGF	Regulates osteoclast differentiation and activation, may recruit osteoclasts for maintenance of normal bone remodeling [52]; promotes ossification via neovascularization or direct effects on bone cells [53]	11.05%
KC	May enhance osteoclast fusion in vitro [54]	5.29%
CD40L	Required for ovariectomy to promote osteoblast proliferation and differentiation, mediate production of M-CSF and RANKL by stromal cells and upregulate osteoclast formation [55]	35.66%
CTLA4	Inhibition may lead to cytokine-mediated increase in bone remodeling [56]	14.18%
Neprilysin	May control proliferation and differentiation of osteoblastic lineage cells and resorption by osteoclasts [57]	0.50%
TROY	Mediates commitment of mesenchymal stem cells to the osteoblastic lineage [58,59]	0.38%
VEGFR1	VEGF promotes osteoclast differentiation by activating VEGFR1 [60]	17.03%
Cystatin C	Inhibits bone resorption; stimulates proliferation of MC3T3-E1 cells [61]	2.16%
DLL 4	Accompanies osteogenic differentiation [62]	2.91%
IL-33	Inhibits osteoclast differentiation and activity by inducing apoptosis [63]; stimulates RANKL expression in MC3T3-E1 cells [64]	21.72%

Table 3
Osteocyte cytokines for which concentration decreased insignificantly with load.

	Role in osteoclast/osteoblast activity	Change with load
AR	Promotes proliferation of preosteoblasts but impedes further differentiation [65]; acts as chemotactic factor for migration of mesenchymal progenitors toward parathyroid hormone-stimulated osteoblasts and osteocytes [66]	−11.43%
I-TAC	Inhibits osteoclast differentiation [67]	−6.34%
G-CSF	Reduces osteoblasts and stimulates osteoclasts in short term [68]	−7.05%
MIP-1 g	Promotes differentiation and survival of osteoclasts [69]	−6.96%
RANTES	Acts as osteoblast chemoattractant and promotes survival [70]	−14.38%
Decorin	Inhibits osteoclast formation; promotes osteoblast differentiation [71]	−14.98%
Dkk-1	Inhibits canonical Wnt/β-catenin signaling; negatively regulates osteoblast function [72]	−17.42%
FIT-3 L	May negatively regulate osteoclast development in pathogenesis of arthritis [73]	−20.30%
Galectin-1	Negatively correlated with osteoclast formation, TRAP secretion and resorption [74]	−0.35%
Galectin-3	Inhibits osteoblast differentiation [75]	−2.56%
B7-1	May negatively regulate generation of bone-resorbing osteoclasts [76]	−5.77%
Chemerin	Mediates osteoblastogenic differentiation of mesenchymal stem cells [77]	−35.44%
Clusterin	Inhibits bone resorption; inhibits bone marrow mesenchymal stem cells from differentiating into osteoblasts [78]	−24.47%
Kremen-1	Functions as Dkk1 receptor and cooperates with Dkk1 to inhibit Wnt/β-catenin signaling [79]	−24.50%
Osteoactivin	Positively regulates osteoblastogenesis [80]; negatively regulates osteoclastogenesis [81]	−24.62%
MMP-2	Supports growth and proliferation of osteoclasts and osteoblasts [82]	−23.34%
sFRP3	Inhibits Wnt signaling; increases osteoblast differentiation but decreases osteoblast proliferation [83,84]	−26.38%

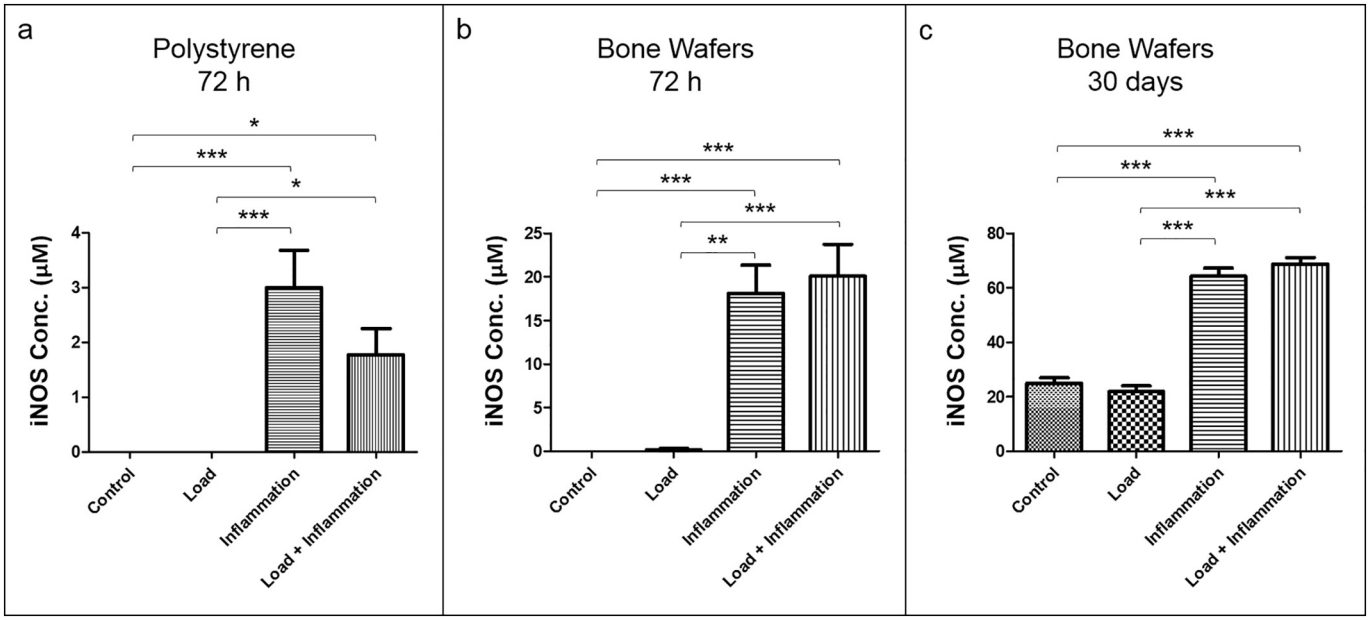

Fig. 9. Results of Griess assays at 72 h and 30 days. a) Osteoclast inducible nitric oxide synthase (iNOS) production on polystyrene at 72 h post-induction. b) Osteoclast iNOS production on bone wafers at 72 h post-induction. c) Osteoclast iNOS production on bone wafers at 30 days post-induction. For all analyses, $n = 9$, and error bars represent standard errors of the means. One asterisk indicates $p \leq 0.05$, two asterisks indicate $p \leq 0.01$ and three asterisks indicate $p \leq 0.001$.

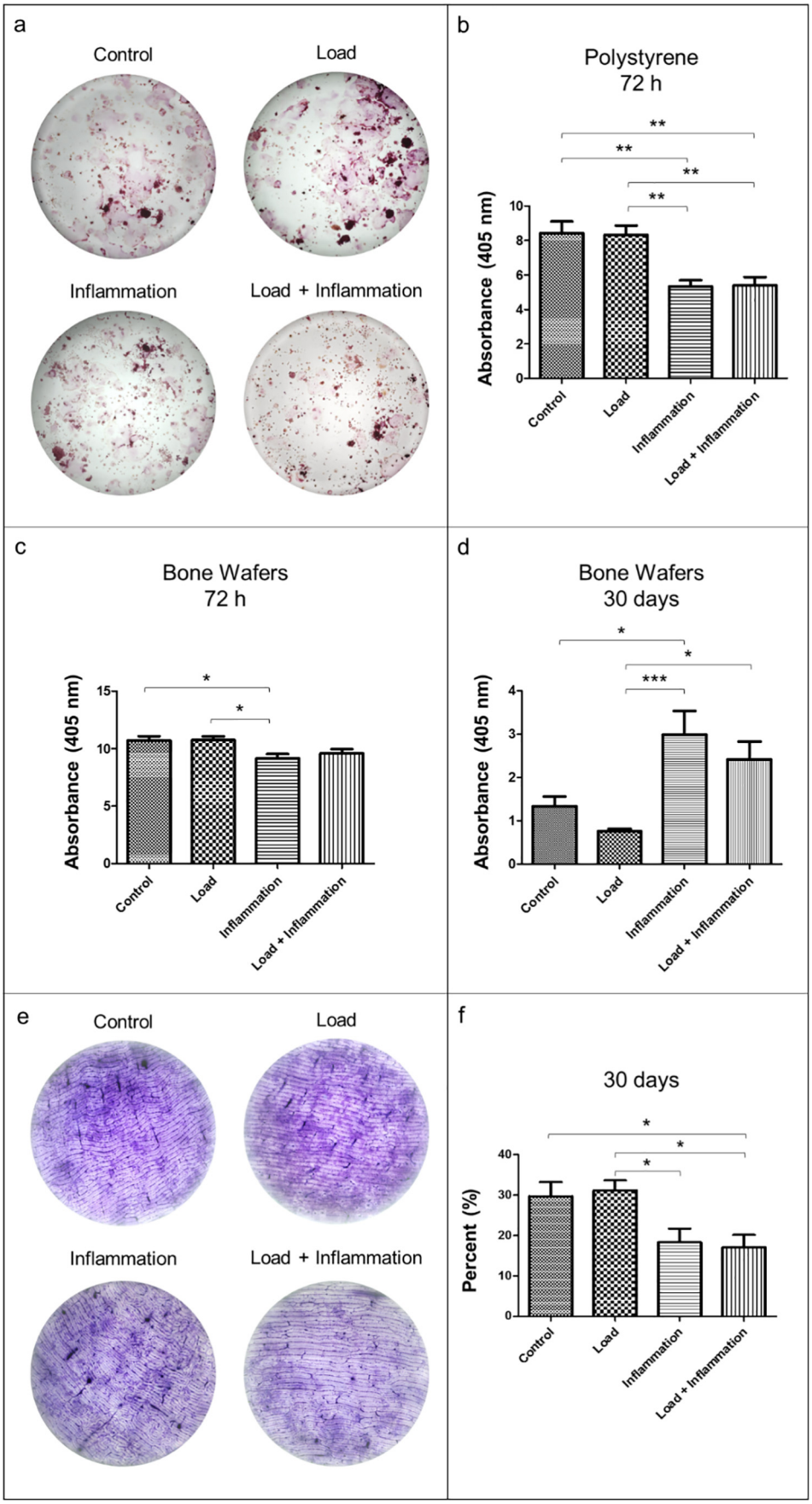

Fig. 10. Osteoclast tartrate-resistant acid phosphatase (TRAP) activity and bone resorption. a) Whole-well images of TRAP stains on polystyrene at 72 h post-induction. b) Absorbance values indicating TRAP activity on polystyrene at 72 h post-induction. c) Absorbance values indicating TRAP activity on bone wafers at 72 h post-induction. d) Absorbance values indicating TRAP activity on bone wafers at 30 days post-induction. e) Whole-wafer images of toluidine blue-stained bone at 30 days post-induction. f) Percentages of bone wafer areas resorbed at 30 days post-induction. Except for the "load" group in f ($n = 8$), all groups in all graphs represent a sample size of 9. Error bars represent standard errors of the means. One asterisk indicates $p \leq 0.05$, two asterisks indicate $p \leq 0.01$ and three asterisks indicate $p \leq 0.001$. (For interpretation of the references to color in this figure legend, the reader is referred to the web version of this article.)

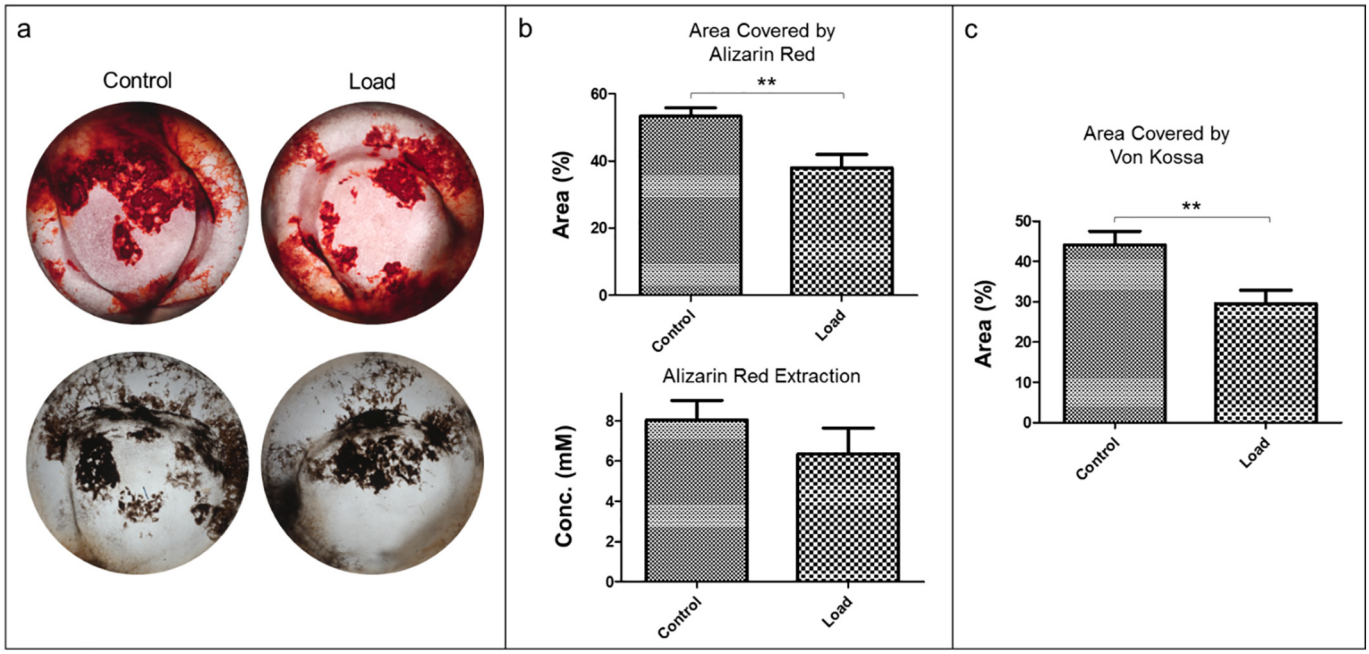

Fig. 11. Osteoblast bone formation at 26 days. a) Whole-well images of bone formation stained with alizarin red (top) and von Kossa (bottom) 26 days post-induction. b) Percentages of cell culture areas covered by alizarin red (top) and concentrations of alizarin red extracted from cultures (bottom). c) Percentages of cell culture areas covered by von Kossa. For all analyses, $n = 9$, and error bars represent standard errors of the means. Two asterisks indicate $p \leq 0.01$. (For interpretation of the references to color in this figure legend, the reader is referred to the web version of this article.)

responsive to inflammatory agents than to soluble factors present within CM from stimulated osteocytes.

3.5. Visualization and quantification of osteoblast bone formation

Results of osteoblast analyses are presented in Fig. 11. The addition of short-term overload to BP-treated osteocyte cultures generated CM that slowed mineralization and resulted in less bone formation than did CM from non-loaded control cultures. Representative images of osteoblasts stained for bone formation by alizarin red (top) and von Kossa (bottom) 26 days post-stimulation are shown in Fig. 11a. Quantification of cell culture area covered by alizarin red indicates that experimental CM decreased bone formation by 28.8% when compared to control CM. While alizarin red extraction results appear to corroborate this finding, no statistically significant difference was found between control and experimental groups (Fig. 11b). Quantification of cell culture area covered by von Kossa indicates that experimental CM decreased bone formation by 33% when compared to control CM (Fig. 11c). In summary, we found that osteoblasts exposed to CM from loaded osteocytes formed significantly less bone than did osteoblasts exposed to CM from non-loaded osteocytes.

4. Conclusions

This study was designed to test our hypothesis that key risk factors—tooth extraction (mechanical trauma) and inflammation associated with infection—cause a defect in bone remodeling, potentially contributing to BRONJ. An inexpensive loading system engineered in-house exposed osteocytes to short-term mechanical trauma within a cell culture incubator that simulates in vivo conditions. This controllable system provided a highly reproducible environment for stimulation. Osteocyte viability and secretion of soluble factors were assessed as functions of load. Cultures of osteoclasts (in the presence or absence of inflammatory agents) and osteoblasts were exposed to osteocyte CM and functional activity quantified. Taken together, our results support the following propositions. In patients who have undergone BP therapy, trauma in the form of tooth extraction initiates the onset of BRONJ. Inflammation associated with bacterial infection attenuates bone resorption by osteoclasts. As such, osteoclasts are unable to adequately remove damaged bone. Ikebe describes a hypothesis for a similar role of osteoclasts in BRONJ and suggests they are unable to degrade necrotic bone, which then accumulates [3]. Additionally, osteocytes respond to overload by altering expression of soluble signals that act on osteoblasts to attenuate bone formation. These defects in bone remodeling can cause buildup of necrotic bone, culminating in BRONJ.

The processes of mechanotransduction and bone turnover are incredibly intricate. As such, multicellular models that represent the bone's physiologic complexity must be developed for the study of remodeling-related disease. These models must allow for the investigation of the aggregate response of osteocytes, osteoclasts and osteoblasts to risk factors. Our major goal was to describe the osteocyte's ability to sense overload and transduce signals to the osteoclasts and osteoblasts in relation to BRONJ. Our model has led to interesting observations that could help us better grasp the pathophysiology of the disease. However, limitations of this work should be considered in future studies. Zhao et al. suggest that osteoclasts and osteoblasts maintain bone homeostasis through physical contact signaling. A bidirectional interaction occurs between osteoclast ephrinB ligands and osteoblast Eph receptors; this facilitates the transition from resorption to osteoclast attenuation and osteoblast bone formation. Subramanian et al. postulate that when local remodeling synergy is compromised, bone cells are unable to respond to injury (i.e. dental extraction) at the site of the lesion, resulting in BRONJ [87,88]. We are presently working to establish osteoclast-osteoblast co-cultures for the study of bidirectional signaling and have determined culture conditions and densities that enable concurrent functional activity of both cell types (data not shown). Additionally, in our current model, the direct effects of BPs on osteoclasts and osteoblasts are not incorporated. Direct exposure to BPs induces osteoclast apoptosis and, at high concentrations, osteoblast apoptosis. It has been suggested that these apoptotic osteoclasts release isopentenyl diphosphate at the surface of the bone to promote oral innate immune responses. Hokugo et al. hypothesize that, following tooth extraction, BP therapy in combination with vitamin D deficiency gives way to tissue damage by neutrophils and cytotoxicity by γδ T

cells, potentially leading to osteonecrosis [89,90]. As such, future models should incorporate both direct and indirect effects of BPs as well as immune system complexities to systematically elucidate the pathways by which BRONJ ensues.

Acknowledgments

The authors would like to thank Catherine E. Seno and Christopher C. Van Vranken for their help making PDMS chips and analyzing images. Funding: This work was supported by the National Science Foundation [CBET 1060990 and EBMS 1700299] and the National Institutes of Health NIDCR [DE022664].

Appendix A. Supplementary data

Supplementary data to this article can be found online at https://doi.org/10.1016/j.bone.2019.07.008.

References

[1] M.H. Abu-Id, P.H. Warnke, J. Gottschalk, I. Springer, J. Wiltfang, Y. Acil, P.A. Russo, T. Kreusch, "Bis-phossy jaws" - high and low risk factors for bisphosphonate-induced osteonecrosis of the jaw, J. Craniomaxillofac. Surg. 36 (2) (2008) 95–103.
[2] E.L. George, Y.-L. Lin, M.M. Saunders, Bisphosphonate-related osteonecrosis of the jaw: a mechanobiology perspective, Bone Rep 8 (2018) 104–109.
[3] T. Ikebe, Pathophysiology of BRONJ: drug-related osteoclastic disease of the jaw, Oral Science International 10 (1) (2013) 1–8.
[4] S. Otto, C. Schreyer, S. Hafner, G. Mast, M. Ehrenfeld, S. Sturzenbaum, C. Pautke, Bisphosphonate-related osteonecrosis of the jaws - characteristics, risk factors, clinical features, localization and impact on oncological treatment, J. Craniomaxillofac. Surg. 40 (4) (2012) 303–309.
[5] J.-W. Kim, M.E.A. Landayan, J.-Y. Lee, J.C.I. Tatad, S.-J. Kim, M.-R. Kim, I.-H. Cha, Role of microcracks in the pathogenesis of bisphosphonate-related osteonecrosis of the jaw, Clin. Oral Investig. 20 (8) (2016) 2251–2258.
[6] S. Rosini, S. Rosini, I. Bertoldi, B. Frediani, Understanding bisphosphonates and osteonecrosis of the jaw: uses and risks, Eur. Rev. Med. Pharmacol. Sci. 19 (17) (2015) 3309–3317.
[7] H.M. Frost, Bone's mechanostat: a 2003 update, Anat Rec A Discov Mol Cell Evol Biol 275 (2) (2003) 1081–1101.
[8] A. Mahnama, M. Tafazzoli-Shadpour, F. Geramipanah, M. Mehdi Dehghan, Verification of the mechanostat theory in mandible remodeling after tooth extraction: animal study and numerical modeling, J. Mech. Behav. Biomed. Mater. 20 (2013) 354–362.
[9] J. You, C.E. Yellowley, H.J. Donahue, Y. Zhang, Q. Chen, C.R. Jacobs, Substrate deformation levels associated with routine physical activity are less stimulatory to bone cells relative to loading-induced oscillatory fluid flow, J. Biomech. Eng. 122 (4) (2000) 387–393.
[10] C. Wittkowske, G.C. Reilly, D. Lacroix, C.M. Perrault, In vitro bone cell models: impact of fluid shear stress on bone formation, Front Bioeng Biotechnol 4 (2016) 87.
[11] R.L. Duncan, C.H. Turner, Mechanotransduction and the functional response of bone to mechanical strain, Calcif. Tissue Int. 57 (5) (1995) 344–358.
[12] C.V.B. Gusmão, W.D. Belangero, How do bone cells sense mechanical loading? Rev. Bras. Ortop. 44 (4) (2015) 299–305.
[13] L.M. McNamara, R.J. Majeska, S. Weinbaum, V. Friedrich, M.B. Schaffler, Attachment of osteocyte cell processes to the bone matrix, Anat Rec (Hoboken) 292 (3) (2009) 355–363.
[14] D.P. Nicolella, D.E. Moravits, A.M. Gale, L.F. Bonewald, J. Lankford, Osteocyte lacunae tissue strain in cortical bone, J. Biomech. 39 (9) (2006) 1735–1743.
[15] Y. Han, S.C. Cowin, M.B. Schaffler, S. Weinbaum, Mechanotransduction and strain amplification in osteocyte cell processes, Proc. Natl. Acad. Sci. U. S. A. 101 (47) (2004) 16689–16694.
[16] A.R. Bonivtch, L.F. Bonewald, D.P. Nicolella, Tissue strain amplification at the osteocyte lacuna: a microstructural finite element analysis, J. Biomech. 40 (10) (2007) 2199–2206.
[17] S.W. Verbruggen, T.J. Vaughan, L.M. McNamara, Strain amplification in bone mechanobiology: a computational investigation of the in vivo mechanics of osteocytes, J. R. Soc. Interface 9 (75) (2012) 2735–2744.
[18] O. Sakaguchi, S. Kokuryo, H. Tsurushima, J. Tanaka, M. Habu, M. Uehara, T. Nishihara, K. Tominaga, Lipopolysaccharide aggravates bisphosphonate-induced osteonecrosis in rats, Int. J. Oral Maxillofac. Surg. 44 (4) (2015) 528–534.
[19] C.E. Chandler, R.K. Ernst, Bacterial lipids: powerful modifiers of the innate immune response, F1000Res 6 (2017) (F1000 Faculty Rev-1334).
[20] Y.-C. Lu, W.-C. Yeh, P.S. Ohashi, LPS/TLR4 signal transduction pathway, Cytokine 42 (2) (2008) 145–151.
[21] G.Q. Hou, C. Guo, G.H. Song, N. Fang, W.J. Fan, X.D. Chen, L. Yuan, Z.Q. Wang, Lipopolysaccharide (LPS) promotes osteoclast differentiation and activation by enhancing the MAPK pathway and COX-2 expression in RAW264.7 cells, Int. J. Mol. Med. 32 (2) (2013) 503–510.
[22] D. Muratsu, D. Yoshiga, T. Taketomi, T. Onimura, Y. Seki, A. Matsumoto, S. Nakamura, Zoledronic acid enhances lipopolysaccharide-stimulated proinflammatory reactions through controlled expression of SOCS1 in macrophages, PLoS One 8 (7) (2013) e67906.
[23] E.M. Palsson-McDermott, L.A. O'Neill, Signal transduction by the lipopolysaccharide receptor, toll-like receptor-4, Immunology 113 (2) (2004) 153–162.
[24] V. Kunzmann, E. Bauer, J. Feurle, F.W. Tony, M. Wilhelm Hans-Peter, Stimulation of γδ T cells by aminobisphosphonates and induction of antiplasma cell activity in multiple myeloma, Blood 96 (2) (2000) 384–392.
[25] E. Yamachika, Y. Matsui, M. Matsubara, T. Matsumura, N. Nakata, N. Moritani, A. Ikeda, H. Tsujigiwa, N. Ohara, S. Iida, The influence of zoledronate and teriparatide on gamma delta T cells in mice, J Dent Sci 12 (4) (2017) 333–339.
[26] R.J. van't Hof, S.H. Ralston, Nitric oxide and bone, Immunology 103 (3) (2001) 255–261.
[27] S. Yang, P. Madyastha, W. Ries, L.L. Key, Characterization of interferon gamma receptors on osteoclasts: effect of interferon gamma on osteoclastic superoxide generation, J. Cell. Biochem. 84 (3) (2002) 645–654.
[28] C.-J. Chen, Y. Shi, A. Hearn, K. Fitzgerald, D. Golenbock, G. Reed, S. Akira, K.L. Rock, MyD88-dependent IL-1 receptor signaling is essential for gouty inflammation stimulated by monosodium urate crystals, J. Clin. Invest. 116 (8) (2006) 2262–2271.
[29] N. Sato, N. Takahashi, K. Suda, M. Nakamura, M. Yamaki, T. Ninomiya, Y. Kobayashi, H. Takada, K. Shibata, M. Yamamoto, K. Takeda, S. Akira, T. Noguchi, N. Udagawa, MyD88 but not TRIF is essential for osteoclastogenesis induced by lipopolysaccharide, diacyl lipopeptide, and IL-1α, J. Exp. Med. 200 (5) (2004) 601–611.
[30] E.L. George, S.L. Truesdell, S.L. York, M.M. Saunders, Lab-on-a-chip platforms for quantification of multicellular interactions in bone remodeling, Exp. Cell Res. 365 (1) (2018) 106–118.
[31] S.L. Truesdell, E.L. George, C.E. Seno, M.M. Saunders, 3D printed loading device for inducing cellular Mechanotransduction via matrix deformation, Exp. Mech., (In press).
[32] F.G. Basso, A.P. Silveira Turrioni, J. Hebling, C.A. de Souza Costa, Zoledronic acid inhibits human osteoblast activities, Gerontology 59 (6) (2013) 534–541.
[33] M.A. Scheper, A. Badros, A.R. Salama, G. Warburton, K.J. Cullen, D.S. Weikel, T.F. Meiller, A novel bioassay model to determine clinically significant bisphosphonate levels, Support Care Cancer 17 (12) (2009) 1553.
[34] E.L. George, Quantifying the roles of stimulated osteocytes and inflammation in bone remodeling (Doctoral dissertation), Retrieved from OhioLink (2019).
[35] F.K.-M. Chan, K. Moriwaki, M.J. De Rosa, Detection of necrosis by release of lactate dehydrogenase activity, Methods Mol. Biol. 979 (2013) 65–70.
[36] B.S. Cummings, R.G. Schnellmann, Measurement of cell death in mammalian cells, Curr Protoc Pharmacol (2004), https://doi.org/10.1002/0471141755.ph0471141208s0471141725-0471141712.0471141758 Chapter 12.
[37] J. Lee, C. Park, H.J. Kim, Y.D. Lee, Z.H. Lee, Y.W. Song, H.-H. Kim, Stimulation of osteoclast migration and bone resorption by C–C chemokine ligands 19 and 21, Exp. Mol. Med. 49 (2017) (e358).
[38] O. Kevorkova, C. Martineau, L. Martin-Falstrault, J. Sanchez-Dardon, L. Brissette, R. Moreau, Low-bone-mass phenotype of deficient mice for the cluster of differentiation 36 (CD36), PLoS One 8 (10) (2013) e77701.
[39] P. Collin-Osdoby, L. Rothe, S. Bekker, F. Anderson, P. Osdoby, Decreased nitric oxide levels stimulate osteoclastogenesis and bone resorption both in vitro and in vivo on the chick chorioallantoic membrane in association with neoangiogenesis, J. Bone Miner. Res. 15 (3) (2000) 474–488.
[40] S.V. Koduru, B.H. Sun, J.M. Walker, M. Zhu, C. Simpson, M. Dhodapkar, K.L. Insogna, The contribution of cross-talk between the cell-surface proteins CD36 and CD47-TSP-1 in osteoclast formation and function, J. Biol. Chem. 293 (39) (2018) 15055–15069.
[41] C.C. Schroeder, J.S. Scariot, J.C. Ribeiro, T.M. Deliberador, A.M. Giovanini, Platelet rich plasma (PRP) produces an atherofibrotic histophenotype during craniofacial bone repair due to changes of immunohistochemical expression of Erk1/2, p38alpha/beta, adiponectin and elevated presence of cells exhibiting B-scavenger receptor (CD36+), Braz. Dent. J. 27 (3) (2016) 243–254.
[42] F. Elefteriou, J.D. Ahn, S. Takeda, M. Starbuck, X. Yang, X. Liu, H. Kondo, W.G. Richards, T.W. Bannon, M. Noda, K. Clement, C. Vaisse, G. Karsenty, Leptin regulation of bone resorption by the sympathetic nervous system and CART, Nature 434 (7032) (2005) 514–520.
[43] E.L. Scheller, K.D. Hankenson, J.S. Reuben, P.H. Krebsbach, Zoledronic acid inhibits macrophage SOCS3 expression and enhances cytokine production, J. Cell. Biochem. 112 (11) (2011) 3364–3372.
[44] A.M. Delany, K.D. Hankenson, Thrombospondin-2 and SPARC/osteonectin are critical regulators of bone remodeling, J Cell Commun Signal 3 (3–4) (2009) 227–238.
[45] K. Kapinas, C.B. Kessler, A.M. Delany, miR-29 suppression of osteonectin in osteoblasts: regulation during differentiation and by canonical Wnt signaling, J. Cell. Biochem. 108 (1) (2009) 216–224.
[46] E.M. Rosset, A.D. Bradshaw, SPARC/osteonectin in mineralized tissue, Matrix Biol. 52–54 (2016) 78–87.
[47] E.M. Rosset, J. Trombetta-eSilva, G. Hepfer, H. Yao, A.D. Bradshaw, SPARC and the N-propeptide of collagen I influence fibroblast proliferation and collagen assembly in the periodontal ligament, PLoS One 12 (2) (2017) e0173209.
[48] B. Lisowska, D. Kosson, K. Domaracka, Lights and shadows of NSAIDs in bone healing: the role of prostaglandins in bone metabolism, Drug Des Dev Ther 12 (2018) 1753–1758.
[49] J. Lee, H.-H. Kim, OP0263 CCL19 and CCL21 Chemokines Enhance Osteoclast Migration and Resorption Activity, Ann. Rheum. Dis. 74 (7) (2015) 171.
[50] Y. Wang, J. Kim, A. Chan, C. Whyne, D. Nam, A two phase regulation of bone

regeneration: IL-17F mediates osteoblastogenesis via C/EBP-β in vitro, Bone 116 (2018) 47–57.
[51] A. Singh, G. Gill, H. Kaur, M. Amhmed, H. Jakhu, Role of osteopontin in bone remodeling and orthodontic tooth movement: a review, Prog. Orthod. 19 (1) (2018) 18.
[52] K. Hu, B.R. Olsen, The roles of vascular endothelial growth factor in bone repair and regeneration, Bone 91 (2016) 30–38.
[53] Y.-Q. Yang, Y.-Y. Tan, R. Wong, A. Wenden, L.-K. Zhang, A.B.M. Rabie, The role of vascular endothelial growth factor in ossification, Int J Oral Sci 4 (2) (2012) 64–68.
[54] M.S. Valerio, B.A. Herbert, D.S. Basilakos, C. Browne, H. Yu, K.L. Kirkwood, Critical role of MKP-1 in lipopolysaccharide-induced osteoclast formation through CXCL1 and CXCL2, Cytokine 71 (1) (2015) 71–80.
[55] J.Y. Li, H. Tawfeek, B. Bedi, X. Yang, J. Adams, K.Y. Gao, M. Zayzafoon, M.N. Weitzmann, R. Pacifici, Ovariectomy disregulates osteoblast and osteoclast formation through the T-cell receptor CD40 ligand, Proc. Natl. Acad. Sci. U. S. A. 108 (2) (2011) 768–773.
[56] A. Rao, J. Mansour, H. Nordquist, M.F. Shaheen, O. Rixe, Increased bone remodeling on patients treated with a CTLA-4 inhibitor: first report of an unknown autoimmune reaction, J. Clin. Oncol. 33 (15_suppl) (2015) e14027.
[57] A.F. Ruchon, M. Marcinkiewicz, K. Ellefsen, A. Basak, J. Aubin, P. Crine, G. Boileau, Cellular localization of neprilysin in mouse bone tissue and putative role in hydrolysis of osteogenic peptides, J. Bone Miner. Res. 15 (7) (2000) 1266–1274.
[58] W. Qiu, Y. Hu, T.E. Andersen, A. Jafari, N. Li, W. Chen, M. Kassem, Tumor necrosis factor receptor superfamily member 19 (TNFRSF19) regulates differentiation fate of human mesenchymal (stromal) stem cells through canonical Wnt signaling and C/EBP, J. Biol. Chem. 285 (19) (2010) 14438–14449.
[59] H. Wu, T.W. Whitfield, J.A.R. Gordon, J.R. Dobson, P.W.L. Tai, A.J. van Wijnen, J.L. Stein, G.S. Stein, J.B. Lian, Genomic occupancy of Runx2 with global expression profiling identifies a novel dimension to control of osteoblastogenesis, Genome Biol. 15 (3) (2014) R52.
[60] S.E. Aldridge, T.W.J. Lennard, J.R. Williams, M.A. Birch, Vascular endothelial growth factor receptors in osteoclast differentiation and function, Biochem. Biophys. Res. Commun. 335 (3) (2005) 793–798.
[61] T. Yasueda, Y. Abe, M. Shiba, Y. Kamo, Y. Seto, A new insight into cystatin C contained in milk basic protein to bone metabolism: effects on osteoclasts and osteoblastic MC3T3-E1 cells in vitro, Animal Sci J 89 (7) (2018) 1027–1032.
[62] M. Alsheikh, A. Abu-Khader, M. Michalicka, R. Pasha, N. Pineault, Impact of osteoblast maturation on their paracrine growth enhancing activity on cord blood progenitors, Eur. J. Haematol. 98 (6) (2017) 542–552.
[63] I.L. Lima, S. Macari, M.F. Madeira, L.F. Rodrigues, P.M. Colavite, G.P. Garlet, F.M. Soriani, M.M. Teixeira, S.Y. Fukada, T.A. Silva, Osteoprotective effects of IL-33/ST2 link to osteoclast apoptosis, Am. J. Pathol. 185 (12) (2015) 3338–3348.
[64] Y. Mine, S. Makihira, Y. Yamaguchi, H. Tanaka, H. Nikawa, Involvement of ERK and p38 MAPK pathways on Interleukin-33-induced RANKL expression in osteoblastic cells, Cell Biol. Int. 38 (5) (2014) 655–662.
[65] L. Qin, J. Tamasi, L. Raggatt, X. Li, J.H. Feyen, D.C. Lee, E. Dicicco-Bloom, N.C. Partridge, Amphiregulin is a novel growth factor involved in normal bone development and in the cellular response to parathyroid hormone stimulation, J. Biol. Chem. 280 (5) (2005) 3974–3981.
[66] J. Zhu, V.A. Siclari, F. Liu, J.M. Spatz, A. Chandra, P. Divieti Pajevic, L. Qin, Amphiregulin-EGFR signaling mediates the migration of bone marrow mesenchymal progenitors toward PTH-stimulated osteoblasts and osteocytes, PLoS One 7 (12) (2013) e50099.
[67] L.F.L. Coelho, G. Magno de Freitas Almeida, F.J.D. Mennechet, A. Blangy, G. Uzé, Interferon-alpha and -beta differentially regulate osteoclastogenesis: role of differential induction of chemokine CXCL11 expression, Proc. Natl. Acad. Sci. U. S. A. 102 (33) (2005) 11917–11922.
[68] S. Li, Q. Zhai, D. Zou, H. Meng, Z. Xie, C. Li, Y. Wang, J. Qi, T. Cheng, L. Qiu, A pivotal role of bone remodeling in granulocyte colony stimulating factor induced hematopoietic stem/progenitor cells mobilization, J. Cell. Physiol. 228 (5) (2013) 1002–1009.
[69] Y. Okamatsu, D. Kim, R. Battaglino, H. Sasaki, U. Späte, P. Stashenko, MIP-1γ promotes receptor activator of NF-κB ligand-induced osteoclast formation and survival, J. Immunol. 173 (3) (2004) 2084–2090.
[70] S. Yano, R. Mentaverri, D. Kanuparthi, S. Bandyopadhyay, A. Rivera, E.M. Brown, N. Chattopadhyay, Functional expression of beta-chemokine receptors in osteoblasts: role of regulated upon activation, normal T cell expressed and secreted (RANTES) in osteoblasts and regulation of its secretion by osteoblasts and osteoclasts, Endocrinology 146 (5) (2005) 2324–2335.
[71] X. Li, W. Ling, S. Khan, S. Yaccoby, Therapeutic effects of intrabone and systemic mesenchymal stem cell cytotherapy on myeloma bone disease and tumor growth, J. Bone Miner. Res. 27 (8) (2012) 1635–1648.
[72] J.S. Butler, D.W. Murray, C.J. Hurson, J. O'Brien, P.P. Doran, J.M. O'Byrne, The role of Dkk1 in bone mass regulation: correlating serum Dkk1 expression with bone mineral density, J. Orthop. Res. 29 (3) (2011) 414–418.
[73] M.N. Svensson, M.C. Erlandsson, I.M. Jonsson, K.M. Andersson, M.I. Bokarewa, Impaired signaling through the Fms-like tyrosine kinase 3 receptor increases osteoclast formation and bone damage in arthritis, J. Leukoc. Biol. 99 (3) (2016) 413–423.
[74] J. Muller, M. Binsfeld, S. Dubois, G. Carmeliet, Y. Beguin, R. Heusschen, J. Caers, Galectin-1 is involved in osteoclast biology, 43rd Annual European Calcified Tissue Society Congress, Bone Abstracts, Rome, Italy, 2016, p. P201.
[75] K. Nakajima, D.H. Kho, T. Yanagawa, Y. Harazono, X. Gao, V. Hogan, A. Raz, Galectin-3 inhibits osteoblast differentiation through notch signaling, Neoplasia 16 (11) (2014) 939–949.
[76] A. Bozec, M.M. Zaiss, R. Kagwiria, R. Voll, M. Rauh, Z. Chen, S. Mueller-Schmucker, R.A. Kroczek, L. Heinzerling, M. Moser, A.L. Mellor, J.-P. David, G. Schett, T cell costimulation molecules CD80/86 inhibit osteoclast differentiation by inducing the IDO/tryptophan pathway, Sci. Transl. Med. 6 (235) (2014) 235ra260.
[77] S. Muruganandan, R. Govindarajan, N.M. McMullen, C.J. Sinal, Chemokine-like receptor 1 is a novel Wnt target gene that regulates mesenchymal stem cell differentiation, Stem Cells 35 (3) (2017) 711–724.
[78] B.M. Abdallah, A.M. Alzahrani, M. Kassem, Secreted Clusterin protein inhibits osteoblast differentiation of bone marrow mesenchymal stem cells by suppressing ERK1/2 signaling pathway, Bone 110 (2018) 221–229.
[79] B. Mao, W. Wu, G. Davidson, J. Marhold, M. Li, B.M. Mechler, H. Delius, D. Hoppe, P. Stannek, C. Walter, A. Glinka, C. Niehrs, Kremen proteins are Dickkopf receptors that regulate Wnt/β-catenin signalling, Nature 417 (2002) 664.
[80] S.M. Abdelmagid, M.F. Barbe, M.C. Rico, S. Salihoglu, I. Arango-Hisijara, A.H. Selim, M.G. Anderson, T.A. Owen, S.N. Popoff, F.F. Safadi, Osteoactivin, an anabolic factor that regulates osteoblast differentiation and function, Exp. Cell Res. 314 (13) (2008) 2334–2351.
[81] G.R. Sondag, T.S. Mbimba, F.M. Moussa, K. Novak, B. Yu, F.A. Jaber, S.M. Abdelmagid, W.J. Geldenhuys, F.F. Safadi, Osteoactivin inhibition of osteoclastogenesis is mediated through CD44-ERK signaling, Exp. Mol. Med. 48 (9) (2016) e257.
[82] R.A. Mosig, O. Dowling, A. DiFeo, M.C.M. Ramirez, I.C. Parker, E. Abe, J. Diouri, A.A. Aqeel, J.D. Wylie, S.A. Oblander, J. Madri, P. Bianco, S.S. Apte, M. Zaidi, S.B. Doty, R.J. Majeska, M.B. Schaffler, J.A. Martignetti, Loss of MMP-2 disrupts skeletal and craniofacial development and results in decreased bone mineralization, joint erosion and defects in osteoblast and osteoclast growth, Hum. Mol. Genet. 16 (9) (2007) 1113–1123.
[83] Y.S. Chung, D.J. Baylink, A.K. Srivastava, Y. Amaar, B. Tapia, Y. Kasukawa, S. Mohan, Effects of secreted frizzled-related protein 3 on osteoblasts in vitro, J. Bone Miner. Res. 19 (9) (2004) 1395–1402.
[84] M. Shahnazari, W. Yao, M. Corr, N.E. Lane, Targeting the Wnt signaling pathway to augment bone formation, Curr Osteoporos Rep 6 (4) (2008) 142–148.
[85] H. Liu, W. Feng, Yimin, J. Cui, S. Lv, T. Hasegawa, B. Sun, J. Li, K. Oda, N. Amizuka, M. Li, Histological evidence of increased osteoclast cell number and asymmetric bone resorption activity in the tibiae of interleukin-6-deficient mice, J. Histochem. Cytochem. 62 (8) (2014) 556–564.
[86] J. Ljusberg, B. Ek-Rylander, G. Andersson, Tartrate-resistant purple acid phosphatase is synthesized as a latent proenzyme and activated by cysteine proteinases, Biochem. J. 343 (Pt 1Pt 1) (1999) 63–69.
[87] G. Subramanian, H.V. Cohen, S.Y.P. Quek, A model for the pathogenesis of bisphosphonate-associated osteonecrosis of the jaw and teriparatide's potential role in its resolution, Oral Surg Oral Med Oral Pathol Oral Radiol Endod 112 (6) (2011) 744–753.
[88] C. Zhao, N. Irie, Y. Takada, K. Shimoda, T. Miyamoto, T. Nishiwaki, T. Suda, K. Matsuo, Bidirectional ephrinB2-EphB4 signaling controls bone homeostasis, Cell Metab. 4 (2) (2006) 111–121.
[89] A. Hokugo, R. Christensen, E.M. Chung, E.C. Sung, A.L. Felsenfeld, J.W. Sayre, N. Garrett, J.S. Adams, I. Nishimura, Increased prevalence of bisphosphonate-related osteonecrosis of the jaw with vitamin D deficiency in rats, J. Bone Miner. Res. 25 (6) (2010) 1337–1349.
[90] D.W. Williams, C. Lee, T. Kim, H. Yagita, H. Wu, S. Park, P. Yang, H. Liu, S. Shi, K.-H. Shin, M.K. Kang, N.-H. Park, R.H. Kim, Impaired bone resorption and woven bone formation are associated with development of osteonecrosis of the jaw-like lesions by bisphosphonate and anti–receptor activator of NF-κB ligand antibody in mice, Am. J. Pathol. 184 (11) (2014) 3084–3093.